Green to Red Electrochromic Fe(II) Metallo-supramolecular Polyelectrolytes Self-Assembled from Fluorescent 2,6-Bis(2-pyridyl)pyrimidine bithiophene

Sandesh Pai,[a] Michael Moos,[b] Maximilian H. Schreck,[b] Christoph Lambert,[b] and Dirk G. Kurth[a,*]

[a]Julius-Maximilians-Universität Würzburg, Chemische Technologie der Materialsynthese, Röntgenring 11, D-97070 Würzburg, Germany

[b]Center for Nanosystems Chemistry, Institut für Organische Chemie, Universität Würzburg, Am Hubland, D-97074 Würzburg

Phone: +49-(0)931-31-82631; Fax: +49-(0)931-31-82109;

*E-Mail: dirk.kurth@matsyn.uni-wuerzburg.de

Supporting Information

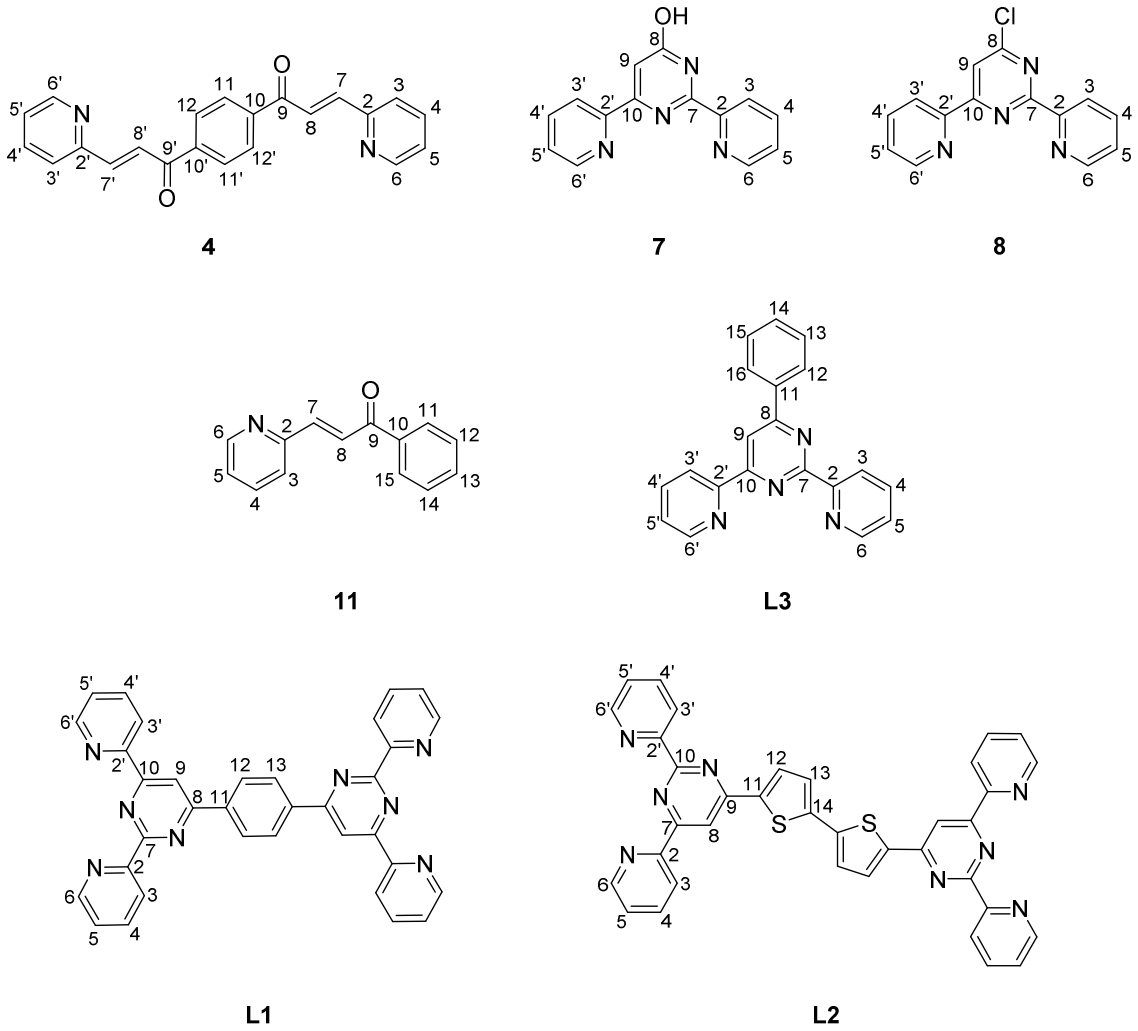

Scheme S1. Numbering scheme for intermediates and ligands **L1-L3**.

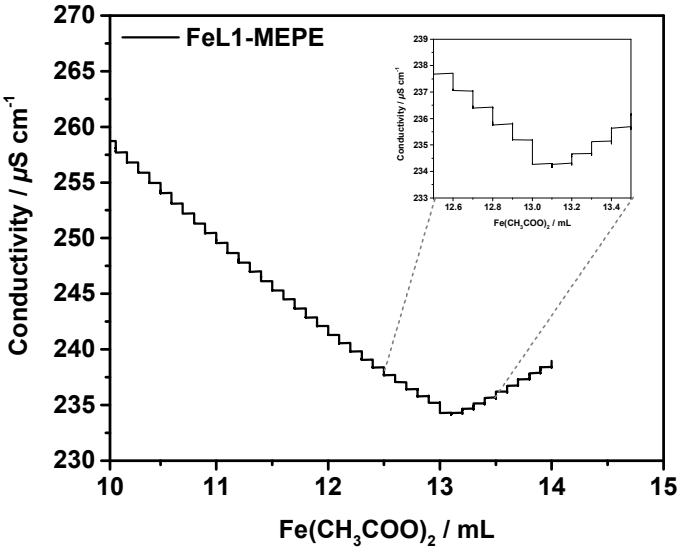

Figure S1. Synthesis of **FeL1-MEPE** by conductometric titration of a solution of ligand (**L1**) in 75% acetic acid (c = 9 mM) with Fe(II) acetate solution (c = 18 mM) in 75% acetic acid at 25 °C, under argon atmosphere and (inset) conductivity minimum at stoichiometry, y = [M]/[L].

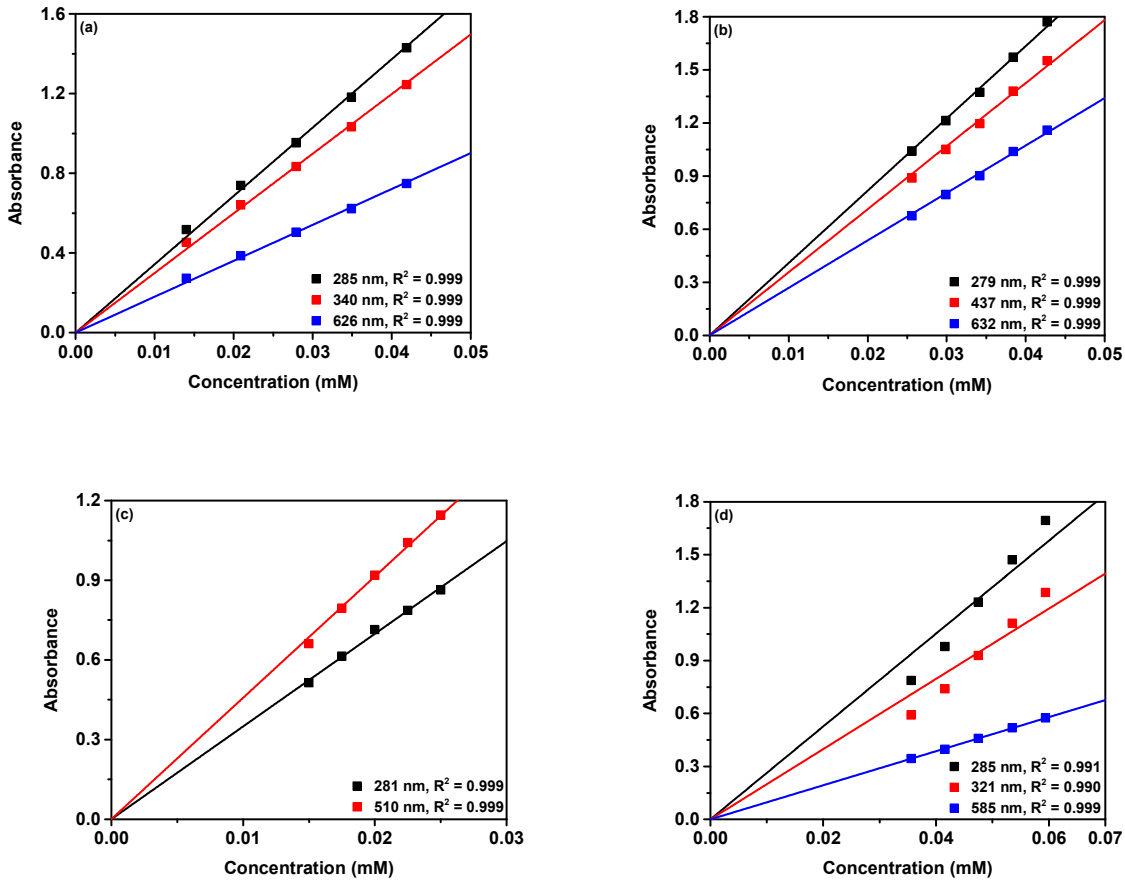

Figure S2. Linear correlation between the concentration and the characteristic peaks of **FeL1-MEPE** (a) in water, **FeL2-MEPE** (b) in ethanol, **CoL2-MEPE** (c) in water and **FL3-MC** (d) in water.

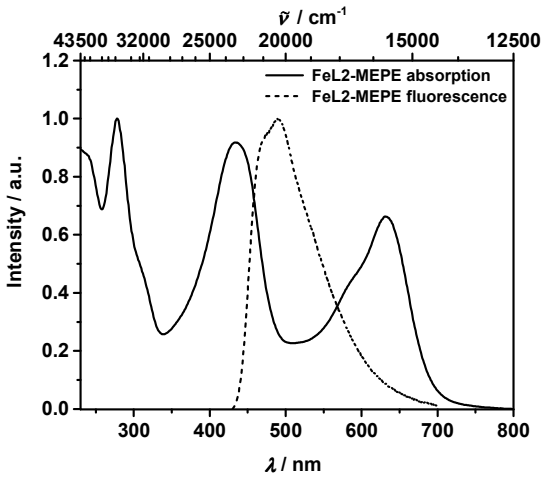

Figure S3. Normalized absorption (solid line) and fluorescence (dotted line) spectrum of **FeL2-MEPE** in MeOH (λ_{exc} = 420 nm).

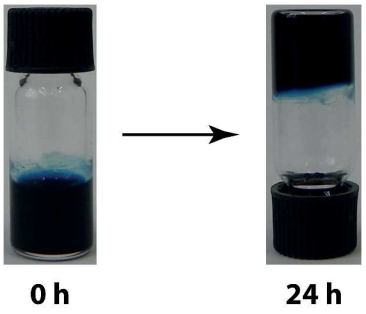

Figure S4. A photographic image of a solution of **FeL1-MEPE** in water (c = 8 mM) at *t* = 0 h, and its formation of viscous gel at ca. *t* = 24 h, upon incubation at 20 °C. Upon turning upside down the viscous gel starts flowing slowly after few minutes (~ 2 – 3 min).

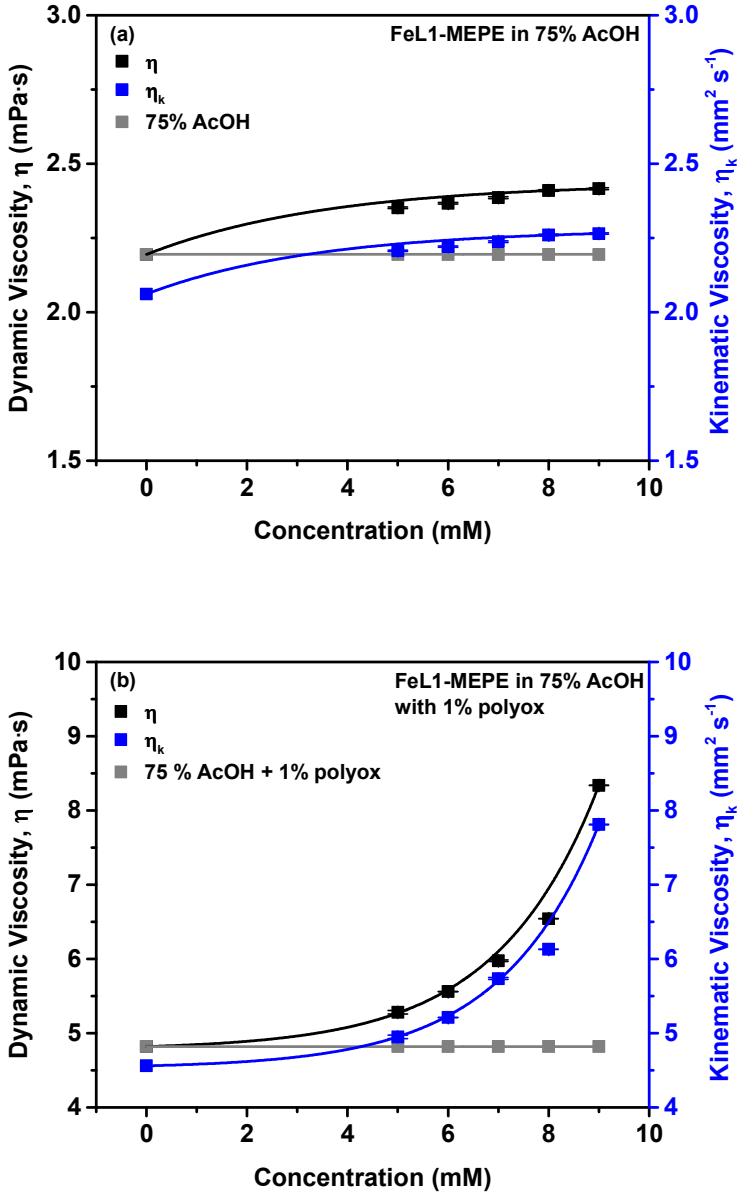

Figure S5. (a) Dynamic and kinematic viscosity of **FeL1-MEPE** in 75% acetic acid as a function of concentration. (b) The effect of water soluble Polyox™ WSR N-80 on the viscosity of **FeL1-MEPE** in 75% acetic acid. The viscosity of 75% acetic acid, and 75% acetic acid with 1% Polyox™ WSR N-80 is shown in grey. The viscosity data points are an average of three independent measurements performed at 20 °C.

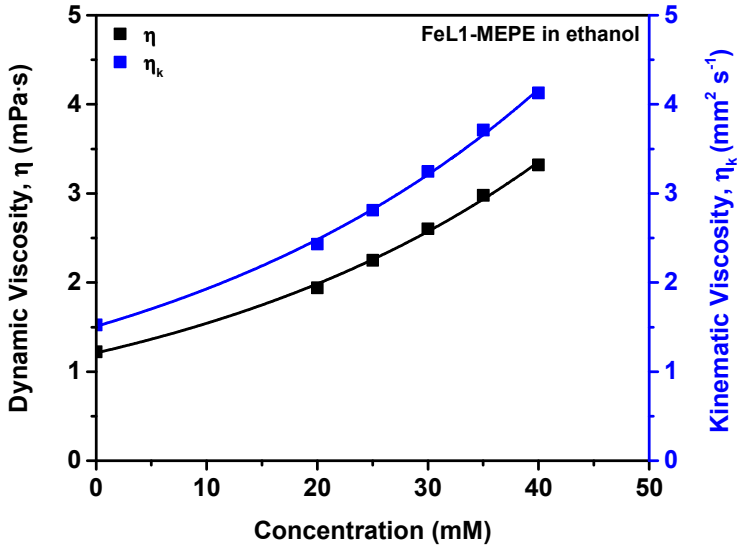

Figure S6. (a) Dynamic and kinematic viscosity of **FeL1-MEPE** in ethanol as a function of concentration. The data on Y-axis at c = 0 mM represents the viscosity of ethanol.

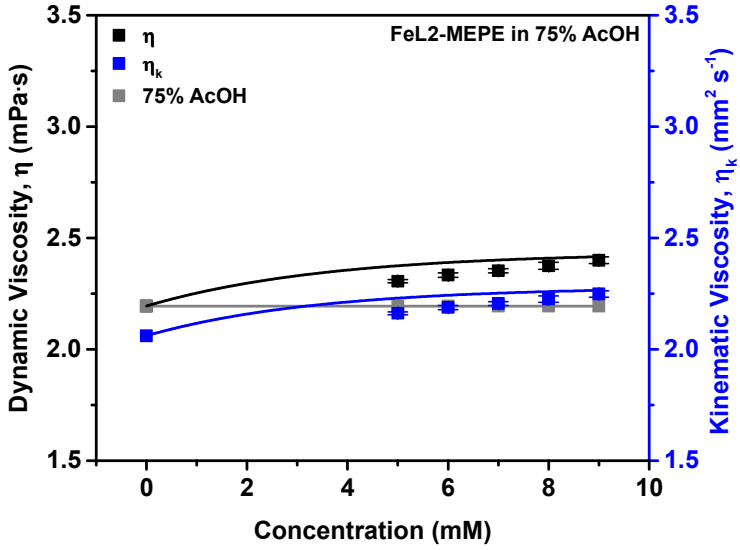

Figure S7. Dynamic and kinematic viscosity of **FeL2-MEPE** in 75% acetic acid as a function of concentration. The viscosity of 75% acetic acid is shown in grey. The viscosity data points are an average of three independent measurements performed at 20 °C.

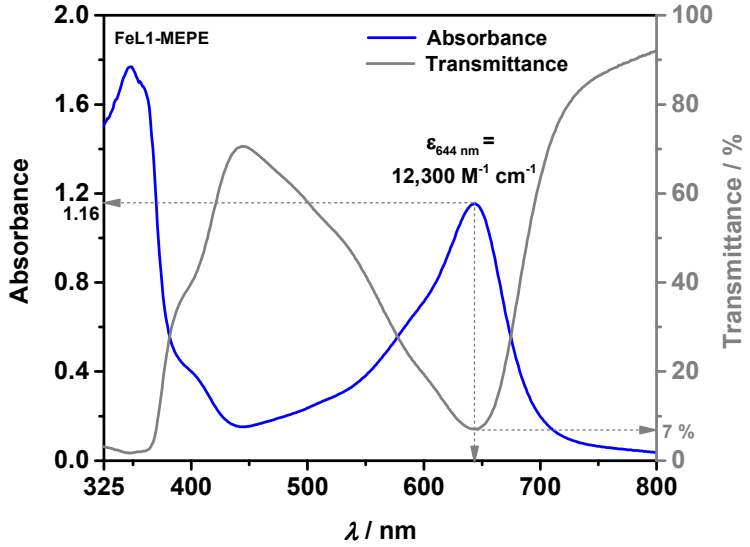

Figure S8. Absorbance and transmittance spectra of **FeL1-MEPE** film on ITO-coated glass (dimension: 1 cm x 2.5 cm) prepared by dip coating using a solution concentration of 30 mM in water, at a withdrawing speed of 100 mm min^{-1}. The molar absorptivity, **ε** of **FeL1-MEPE** amounts to 12,300 $M^{-1}{\cdot}cm^{-1}$.

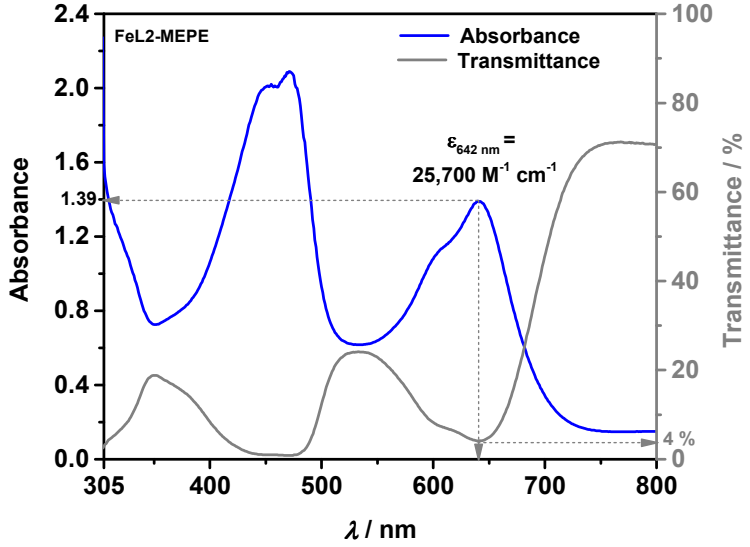

Figure S9. Absorbance and transmittance spectra of **FeL2-MEPE** film on ITO-coated glass (dimension: 1 cm x 2.5 cm) prepared by dip coating using a solution concentration of 14 mM in ethanol, at a withdrawing speed of 100 mm min^{-1}. The molar absorptivity, **ε** of **FeL2-MEPE** amounts to 25,700 $M^{-1}{\cdot}cm^{-1}$.

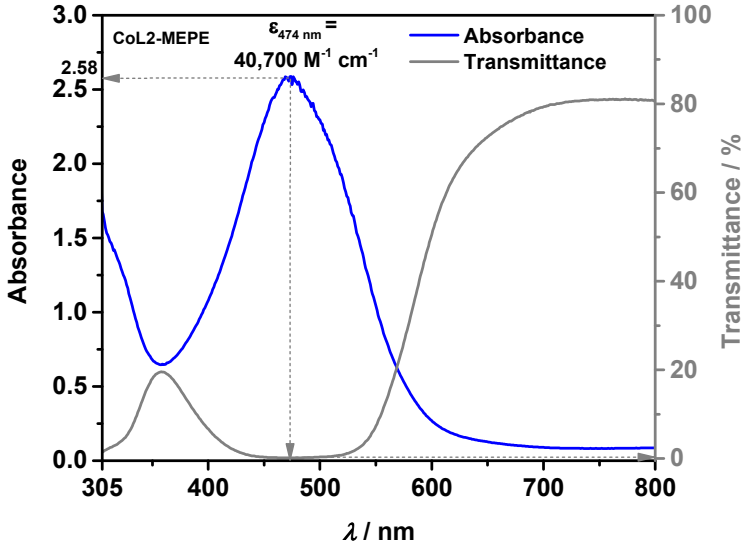

Figure S10. Absorbance and transmittance spectra of **CoL2-MEPE** film on ITO-coated glass (dimension: 1 cm x 2.5 cm) prepared by dip coating using a solution concentration of 14 mM in water, at a withdrawing speed of 100 mm min^{-1}. The molar absorptivity, ε of **CoL2-MEPE** amounts to 40,700 $M^{-1}{\cdot}cm^{-1}$.

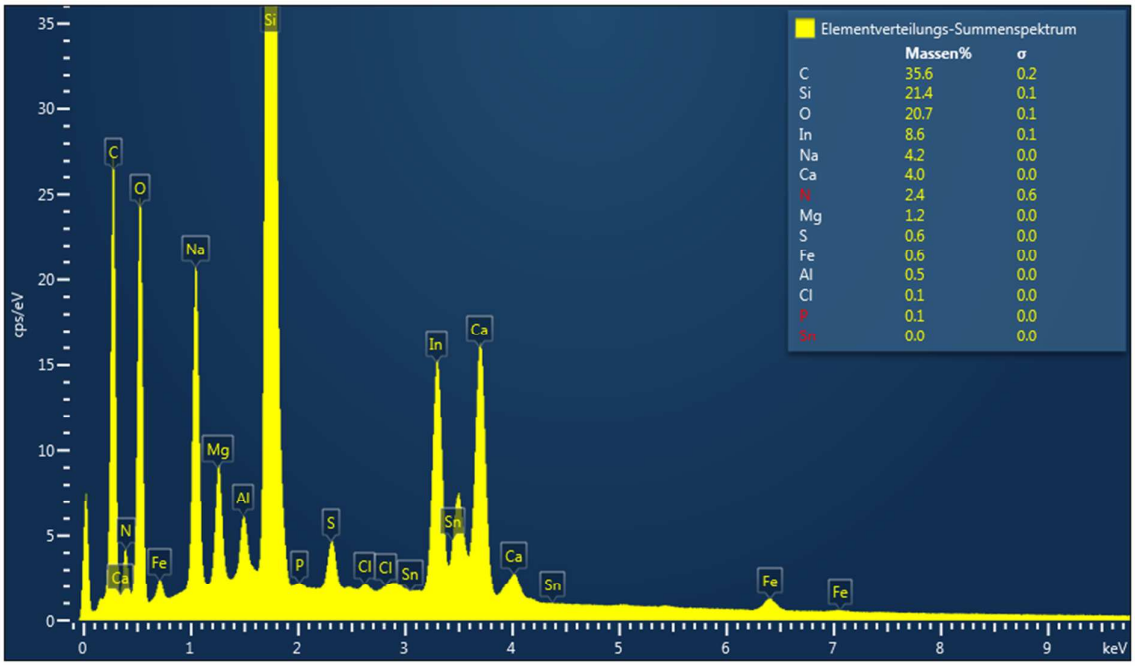

Figure S11. Energy-dispersive X-ray (EDX) spectrum of **FeL2-MEPE** film on ITO-coated glass with calculated mass percentages of the detected elements.

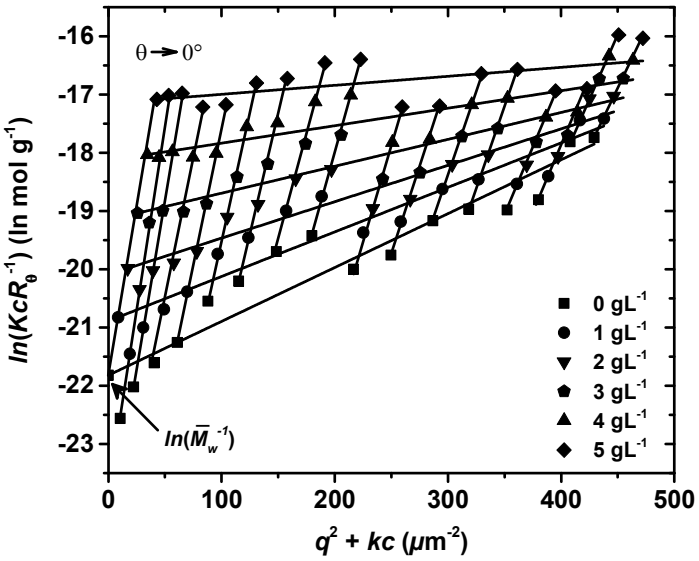

Figure S12. Guinier-Zimm plot of **FeL2-MEPE** in ethanol at 23 °C. The Rayleigh ratio, R_θ, is measured with respect to five solution concentrations (1 – 5 g L^{-1}) and from 16 different angle positions of the detectors, in the range from 20° and 144°. The scaling factor k of the Zimm plot is set to 8.58 L g^{-1} μm^{-2}. The $ln(kcR_\theta^{-1})$ values are extrapolated to $\theta \rightarrow 0$, that is $q^2 \rightarrow 0$, and $c \rightarrow 0$.

Theory: In the static light scattering (SLS), **Fe-MEPE** solutions at different concentrations (c = 1 – 5 g L^{-1}) were prepared in order to calculate the weight average molar mass, $\bar{M}_w$, and the radius of gyration, R_g. The intensity of the scattered light depends on the concentration, c, and the scattering angle, θ, which results in different Rayleigh ratios, R_θ. The R_θ is plotted *via* a Zimm plot according to the equation 1:[1-3]

$$\frac{Kc}{R_\theta} = \frac{1}{\bar{M}_w\left(1 - \frac{1}{3}R_g^2 q^2\right)} + 2A_2 c \qquad (1)$$

where, A_2 is the second virial coefficient. The static light scattering measurements were evaluated by extrapolating the KcR_θ^{-1} values to an interference-free condition, which is $\theta \rightarrow 0$, and leads to the extrapolation of the scattering vector, $q^2 \rightarrow 0$. Also, on the other hand the values are extrapolated to an interaction-free condition, which is $c \rightarrow 0$. As a result, the

Zimm plot is carried out considering the Guinier's method.[4, 5] Moreover, Guinier and Fournet[4, 6] showed that the scattering vector can be approximated over a wide range of q^2 values by equation 2:

$$1 - \frac{1}{3}R_g^2 q^2 = e^{-\frac{1}{3}R_g^2 q^2} \qquad (2)$$

With this approximation, Wesslau[4, 7] proposed the Guinier-Zimm plot based on the equation 3:

$$ln\left(\frac{Kc}{R_\theta}\right) = ln\left(\frac{1}{\bar{M}_w\left(e^{-\frac{1}{3}R_g^2 q^2}\right)} + 2A_2 c\right) \qquad (3)$$

where, $ln(KcR_\theta^{-1})$ is plotted *vs*. $(q^2 + kc)$, as shown in Figure S10 for **FeL2-MEPE**. k is an arbitrary constant, a scaling factor which is freely selectable.

Using the intercept of the extrapolation curve, $q^2 \rightarrow 0$, the weight average molar mass, $\bar{M}_w$, can be estimated by equation 4:

$$\lim_{\substack{q^2 \rightarrow 0 \\ c \rightarrow 0}} \left(ln\left(\frac{Kc}{R_\theta}\right)\right) = ln\left(\frac{1}{\bar{M}_w}\right) \qquad (4)$$

The radius of gyration, R_g, is defined as the squared distance between a point of a polymer and the center of mass, r_i, and is given by equation 5:

$$\langle R_g^2 \rangle_z = \frac{1}{N}\sum_{i=1}^{N} |r_i|^2 \qquad (5)$$

R_g, can also be obtained from the slope of the extrapolated curve of $ln(KcR_\theta^{-1})$ to $c \rightarrow 0$:

$$\frac{d\left(\lim_{c \rightarrow 0}\left(ln\left(\frac{Kc}{R_\theta}\right)\right)\right)}{d(q^2)} = \frac{r_g^2}{3} \qquad (6)$$

Also, the second virial coefficient, A_2, can be estimated from the slope of the extrapolated curve, $q^2 \rightarrow 0$:[1, 2, 4]

$$\frac{d\left(\lim_{q^2 \to 0}\left(\frac{Kc}{R_\theta}\right)\right)}{dc} \cdot k = 2A_2 \qquad (7)$$

Determination of hydrodynamic radii.

A dynamic Zimm plot is generated by measuring the diffusion coefficients, D, and extrapolating the values in the same way as the KcR_θ^{-1} values, as shown in the Guinier-Zimm plot (Figure S11), to an interference-free condition, that is $\theta \rightarrow 0$, which leads to an extrapolation of the scattering vector, $q^2 \rightarrow 0$, and to an interaction-free condition, that is $c \rightarrow 0$. The extrapolation leads to the diffusion coefficient, D_0. Using this D_0, the hydrodynamic radii, R_h, is calculated.[1]

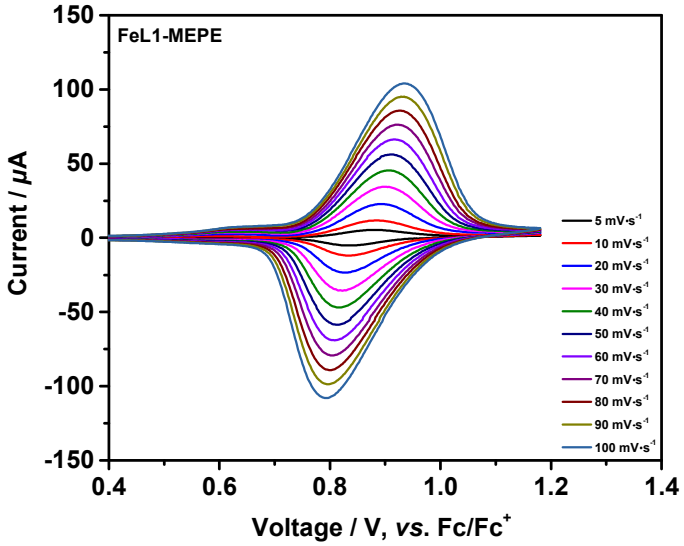

Figure S13. Cyclic voltammogram of **FeL1-MEPE** film on ITO-coated glass (dimension: 0.7 cm x 2.5 cm) at different scan rates (5 to 100 $mV \cdot s^{-1}$) in an electrolyte solution of TBAH (0.2 M) in anhydrous dichloromethane using a platinum wire as counter electrode (CE), and Ag/AgCl as reference electrode (RE).

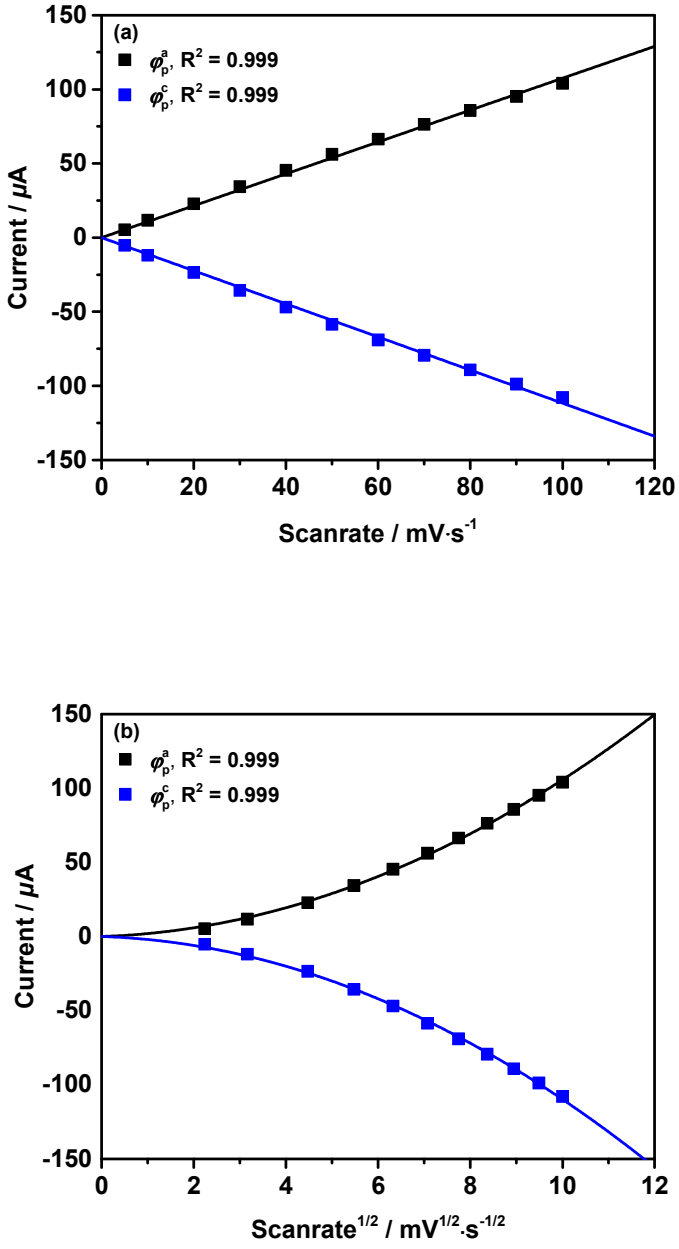

Figure S14. (a) Linear increase of the anodic (φ^a) and cathodic (φ^c) peak currents of **FeL1-MEPE** film on ITO-coated glass as a function of scan rate. (b) Anodic and cathodic peak currents of **FeL1-MEPE** film as a function of square root of the scan rate.

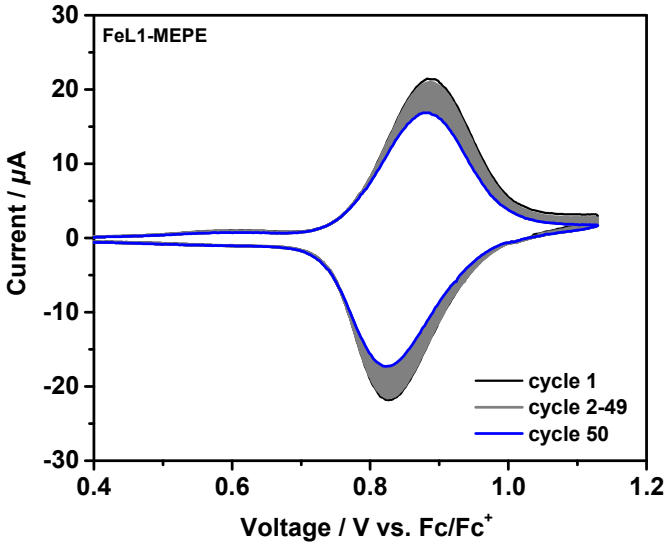

Figure S15. Redox stability of **FeL1-MEPE** on ITO-coated glass examined by cyclic voltammetry after 1 (black) and 50 (blue) redox cycles at a scan rate of 20 $mV \cdot s^{-1}$ at room temperature.

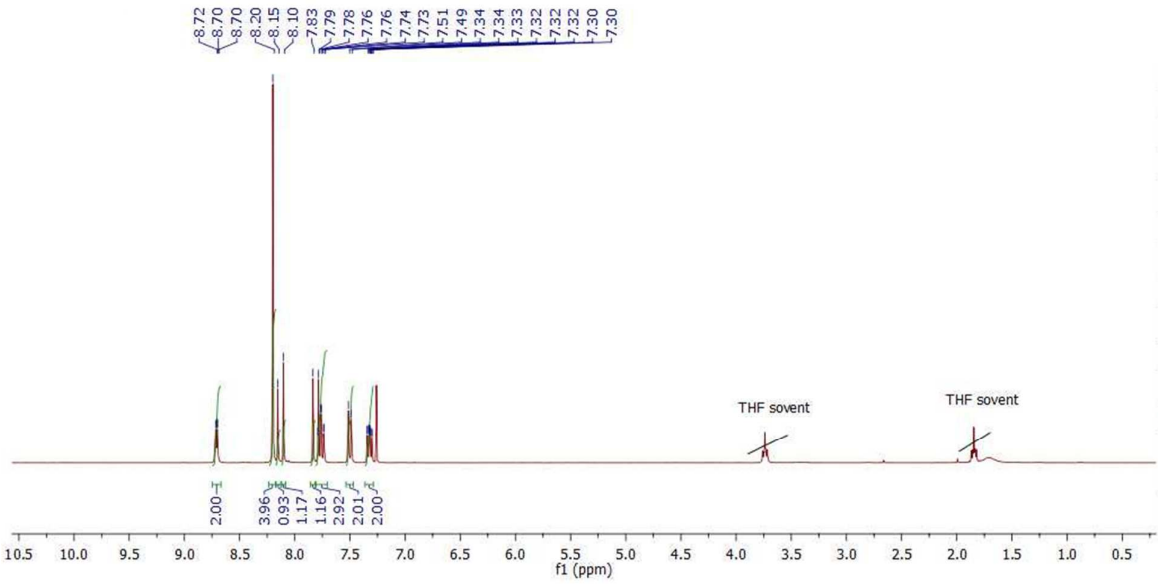

Figure S16. ^{1}H NMR spectrum of compound **4** in $CDCl_3$.

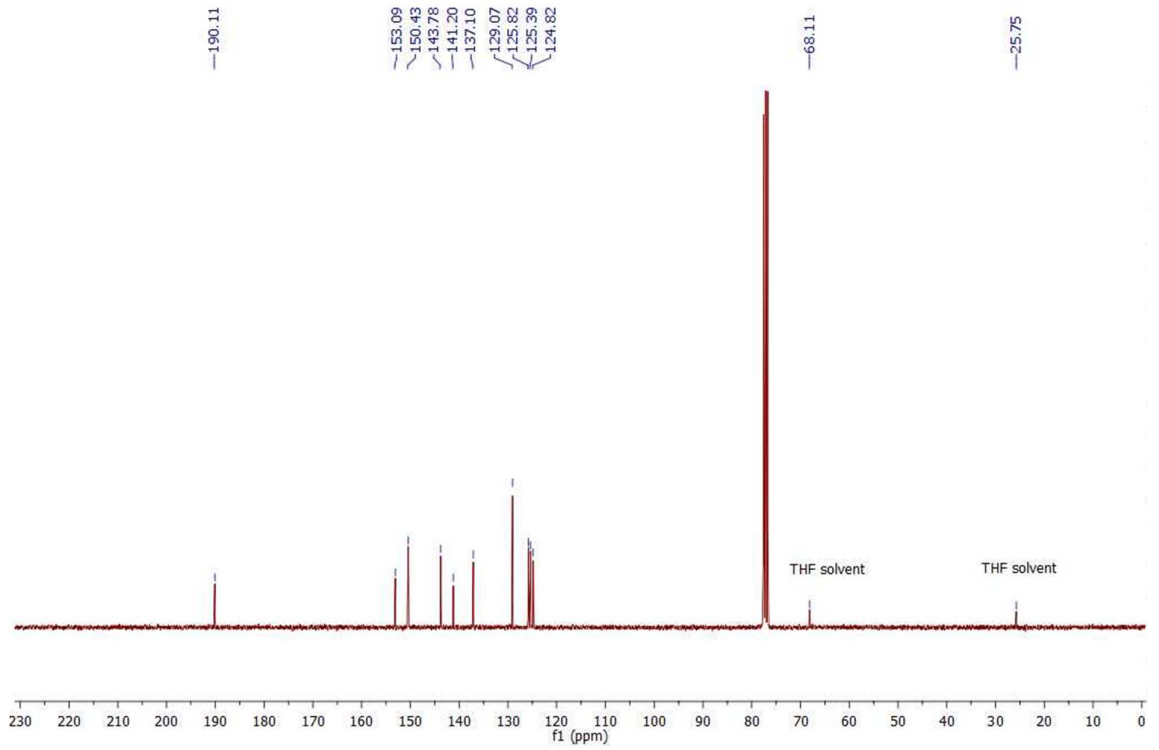

Figure S17. ^{13}C NMR spectrum of compound **4** in $CDCl_3$.

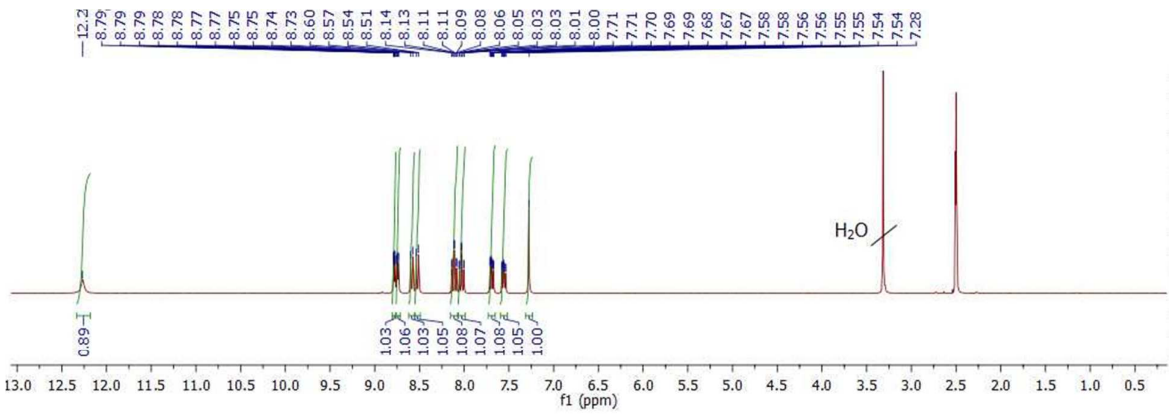

Figure S18. ^{1}H NMR spectrum of compound **7** in DMSO-d_6.

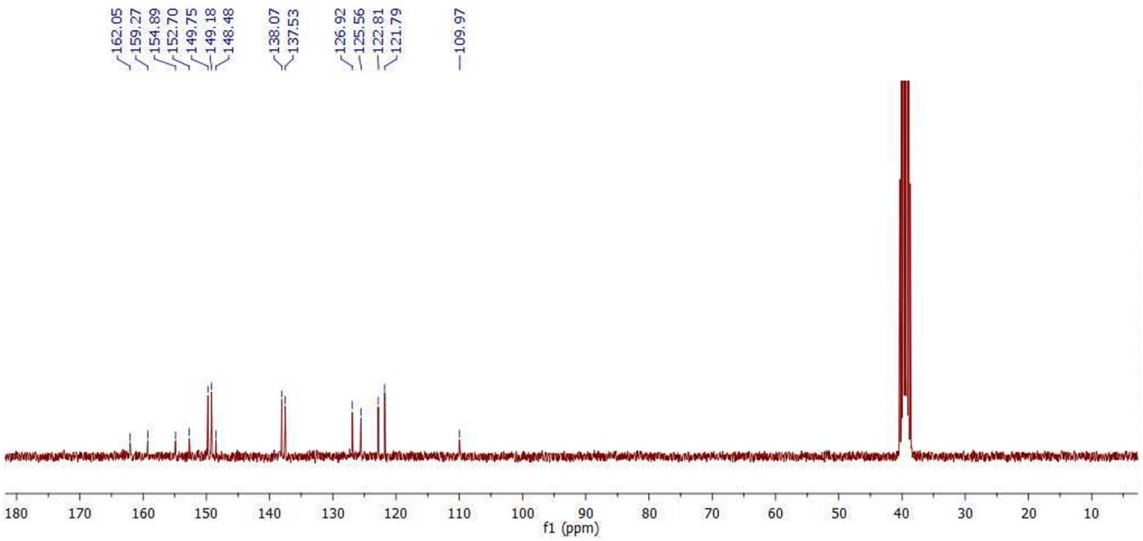

Figure S19. ^{13}C NMR spectrum of compound **7** in DMSO-d_6.

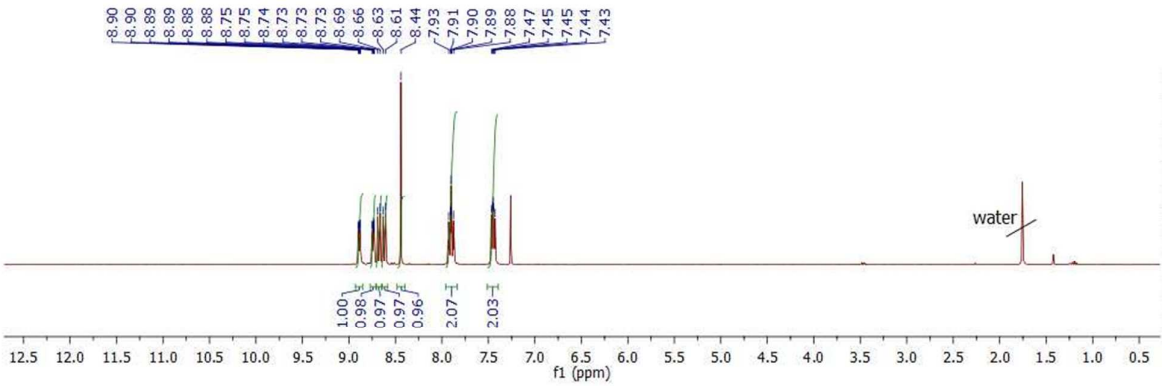

Figure S20. ^{1}H NMR spectrum of compound **8** in $CDCl_3$.

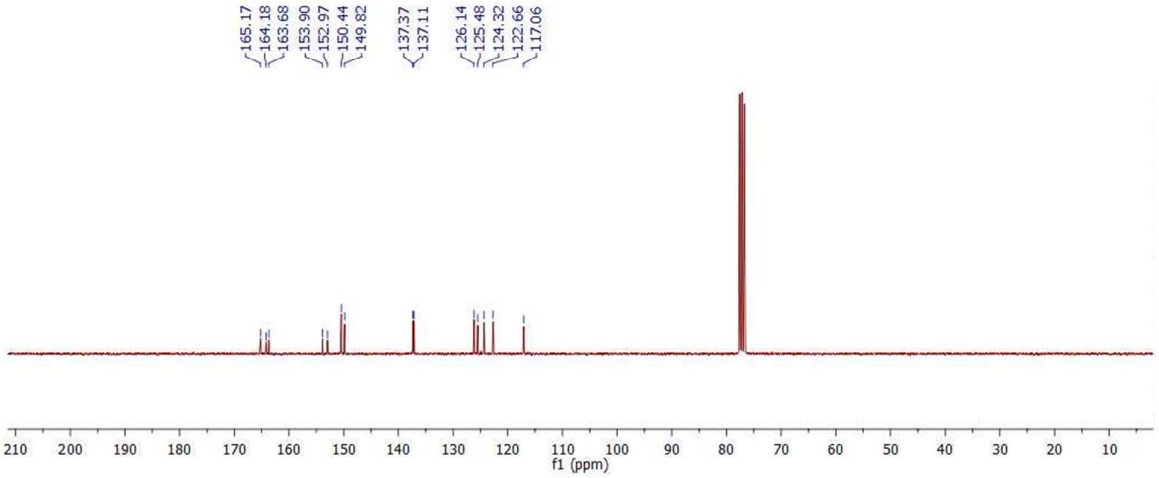

Figure S21. ^{13}C NMR spectrum of compound **8** in $CDCl_3$.

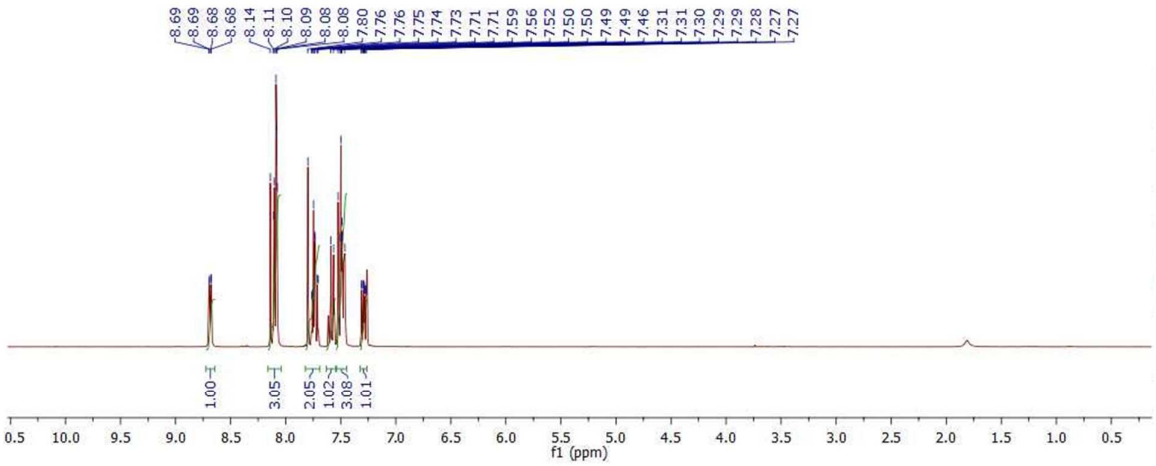

Figure S22. ^{1}H NMR spectrum of compound **11** in $CDCl_3$.

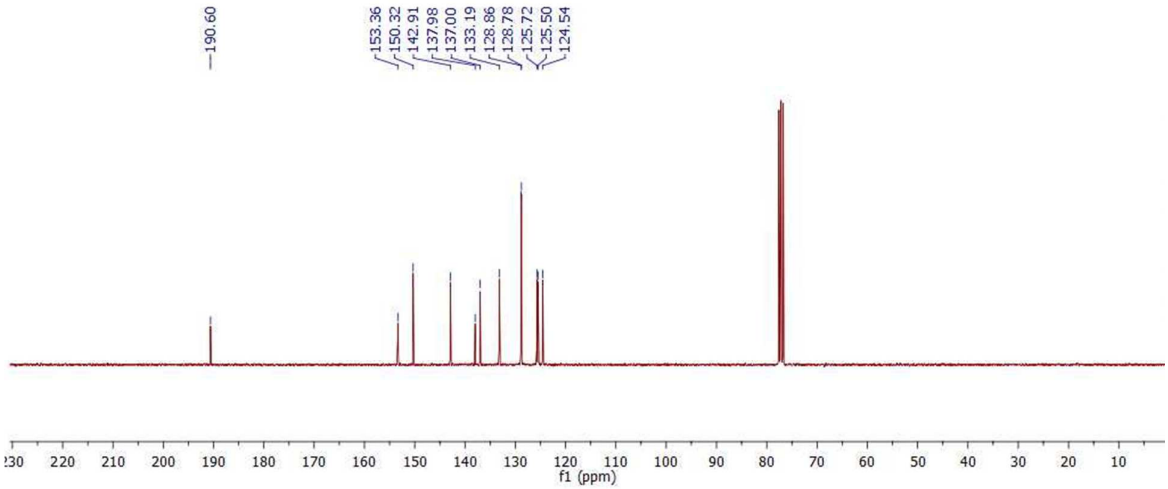

Figure S23. ^{13}C NMR spectrum of compound **11** in $CDCl_3$.

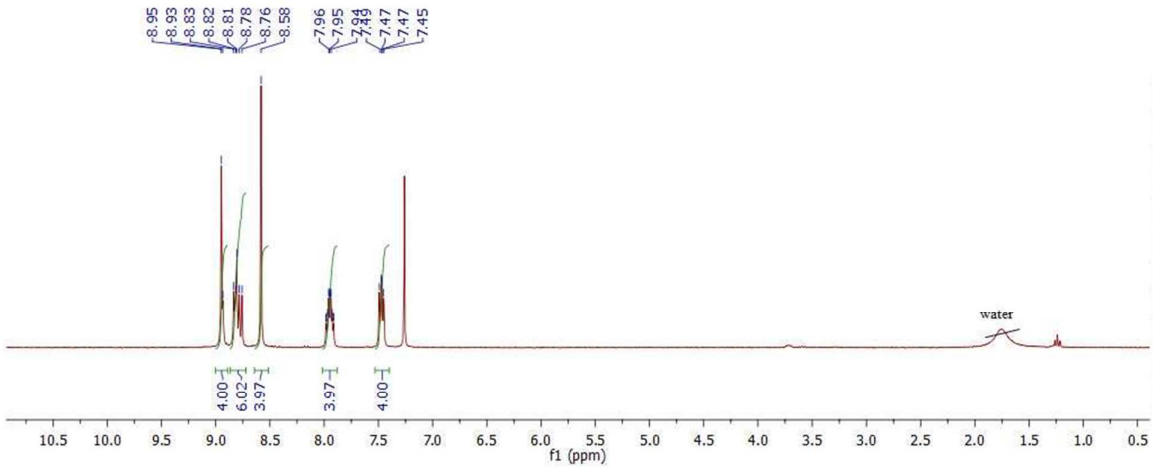

Figure S24. ^{1}H NMR spectrum of ligand **L1** in $CDCl_3$.

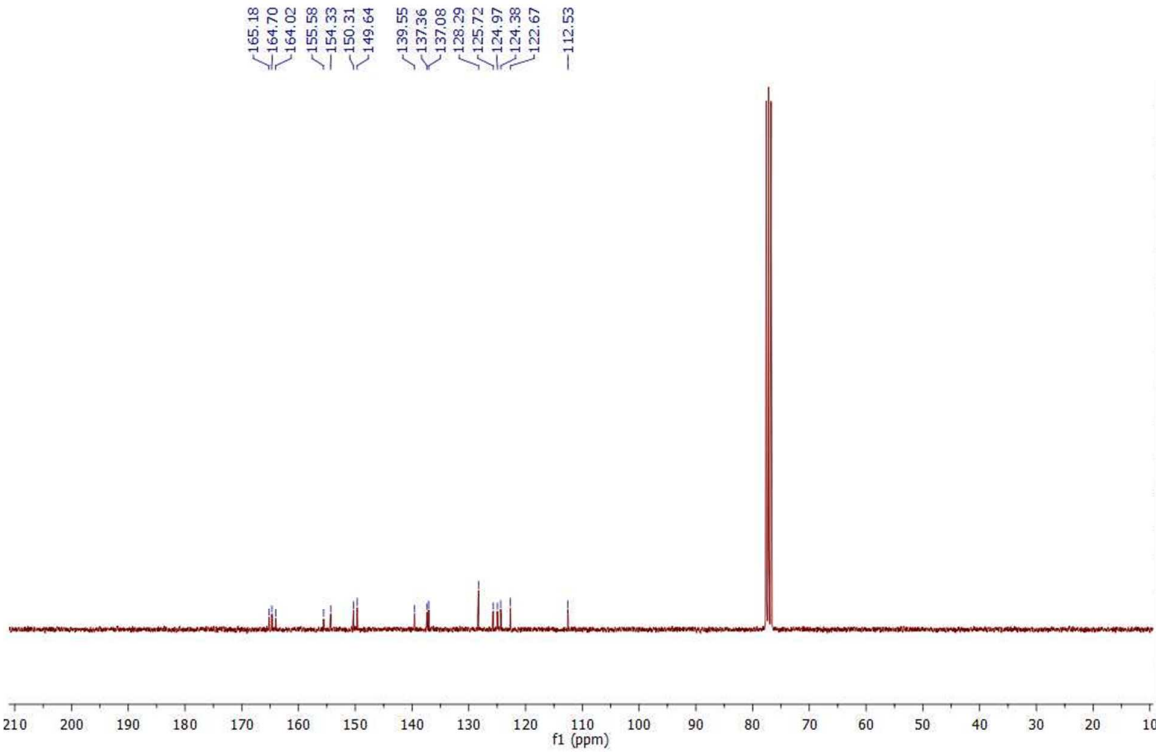

Figure S25. ^{13}C NMR spectrum of ligand **L1** in $CDCl_3$.

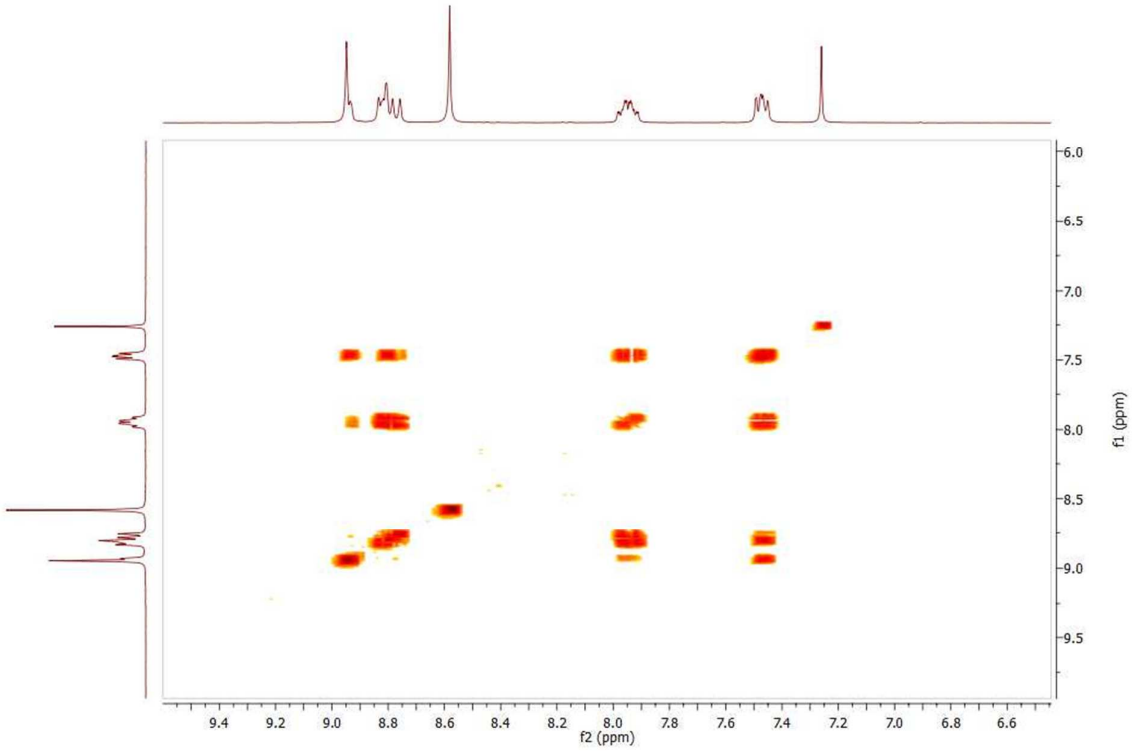

Figure S26. $^{1}H - {}^{1}H$ COSY NMR spectrum of ligand **L1** in $CDCl_3$.

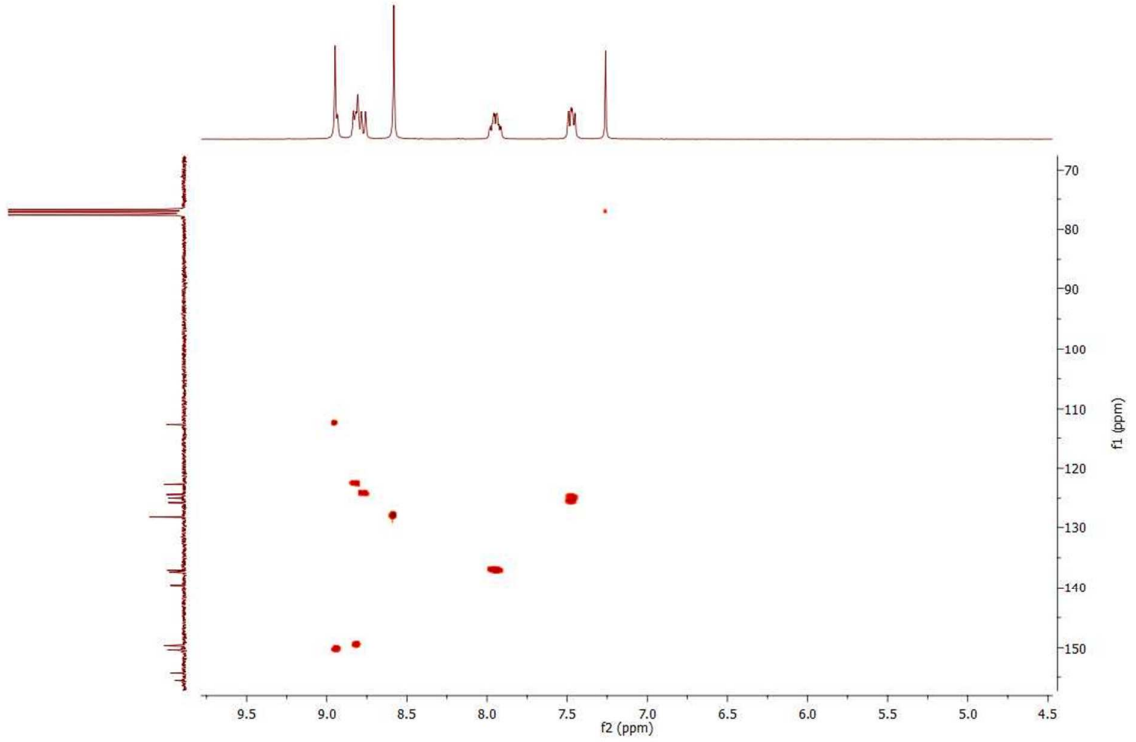

Figure S27. $^{1}H - {}^{13}C$ HSQC NMR spectrum of ligand **L1** in $CDCl_3$.

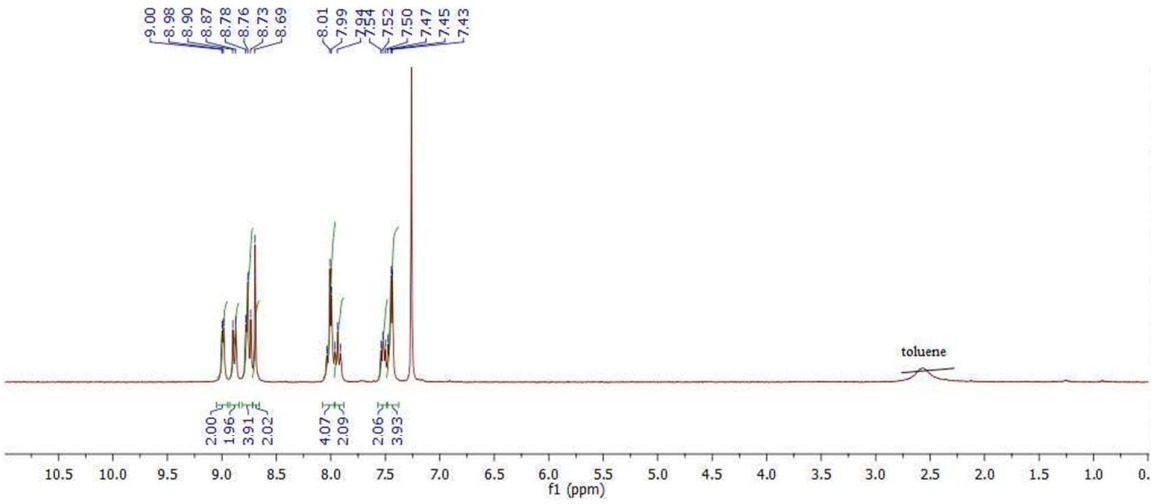

Figure S28. ^{1}H NMR spectrum of ligand **L2** in $CDCl_3$.

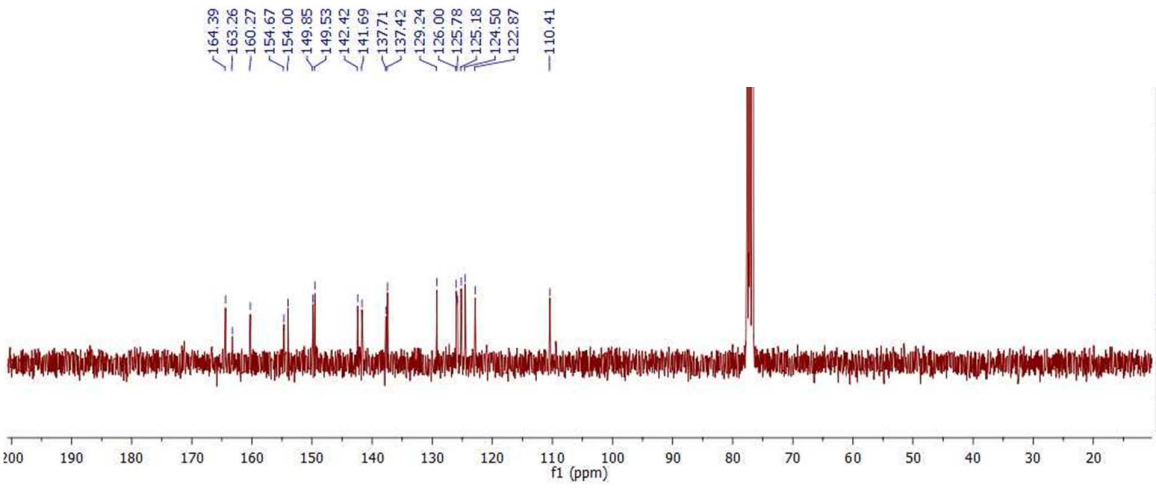

Figure S29. ^{13}C NMR spectrum of ligand **L2** in $CDCl_3$.

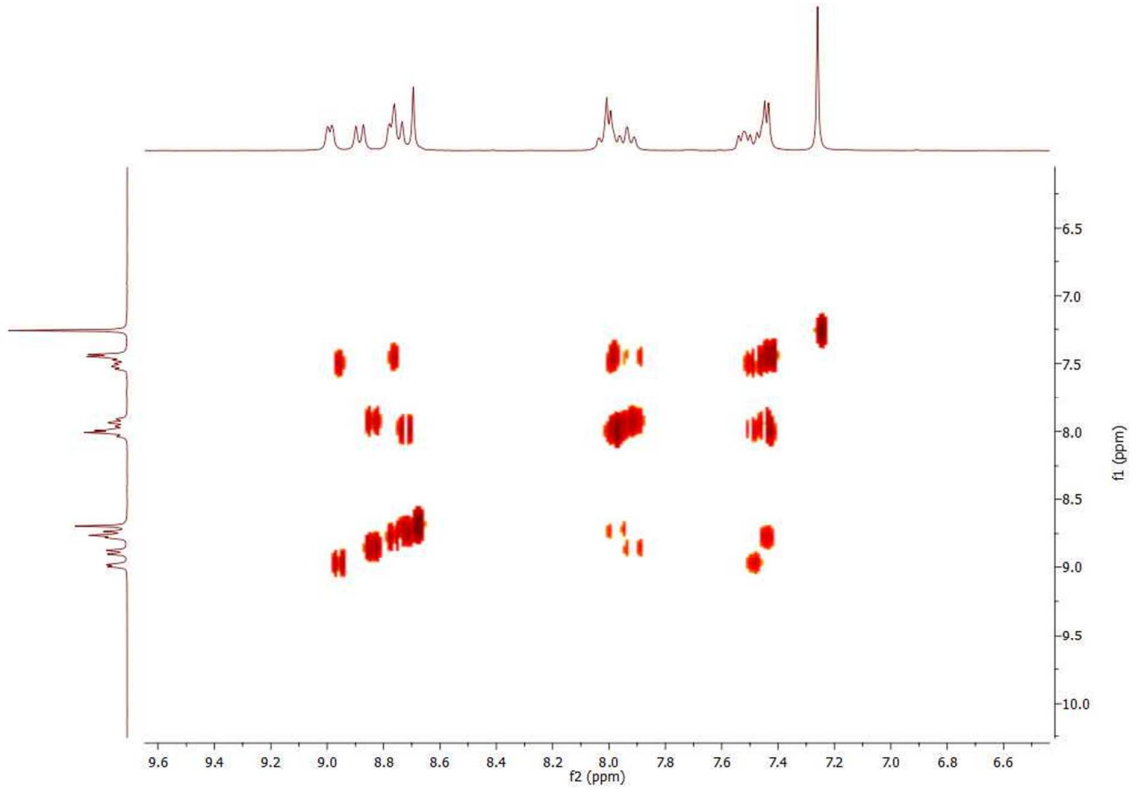

Figure S30. ^{1}H – ^{1}H COSY NMR spectrum of ligand **L2** in $CDCl_3$.

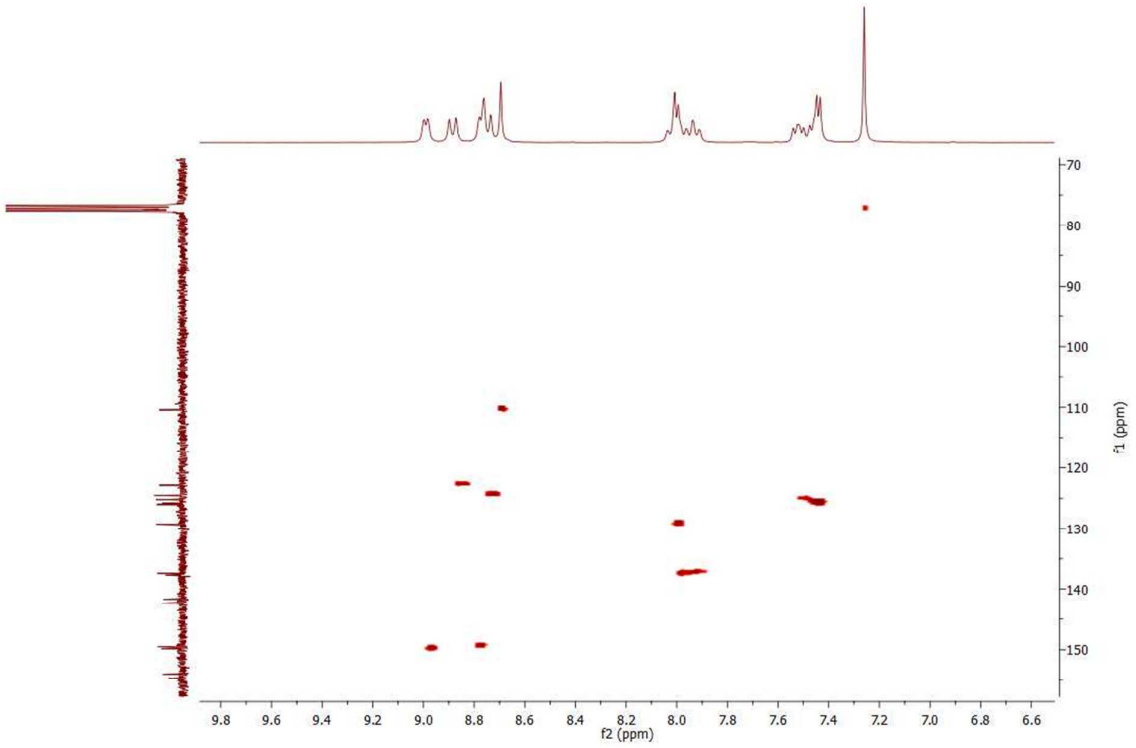

Figure S31. ^{1}H – ^{13}C HSQC NMR spectrum of ligand **L2** in $CDCl_3$.

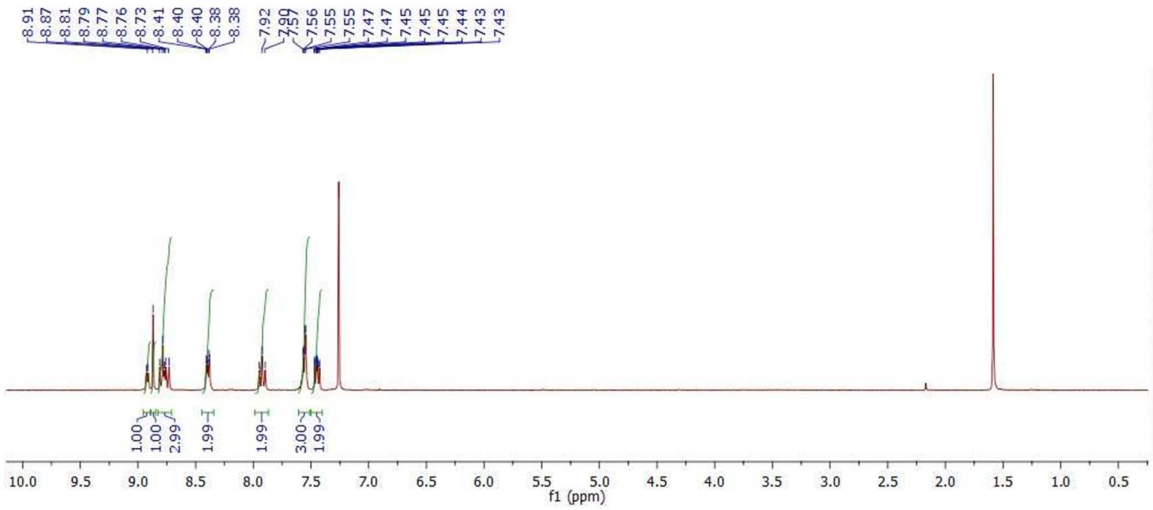

Figure S32. ^{1}H NMR spectrum of ligand **L3** in $CDCl_3$.

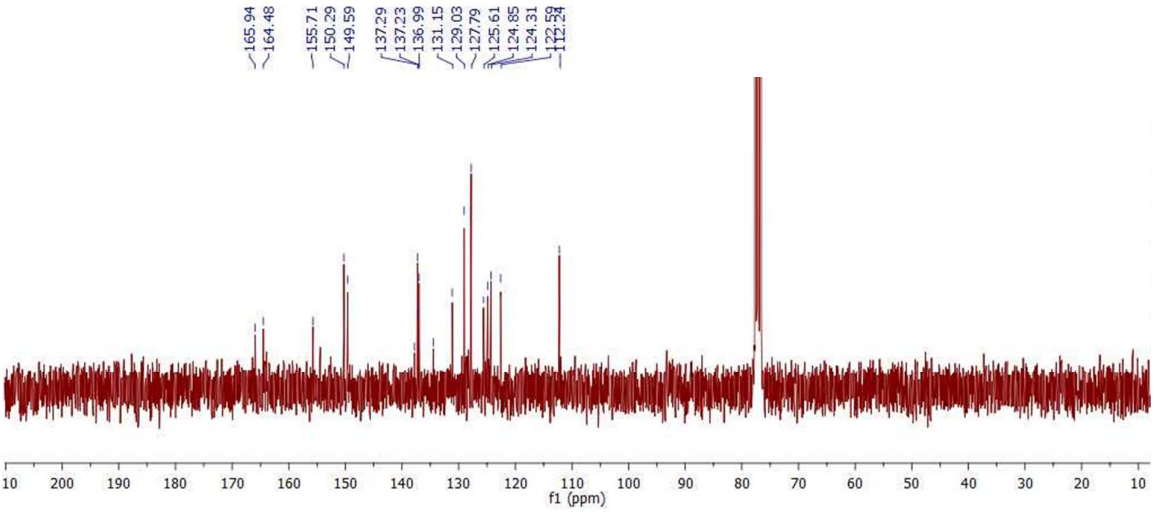

Figure S33. ^{13}C NMR spectrum of ligand **L3** in $CDCl_3$.

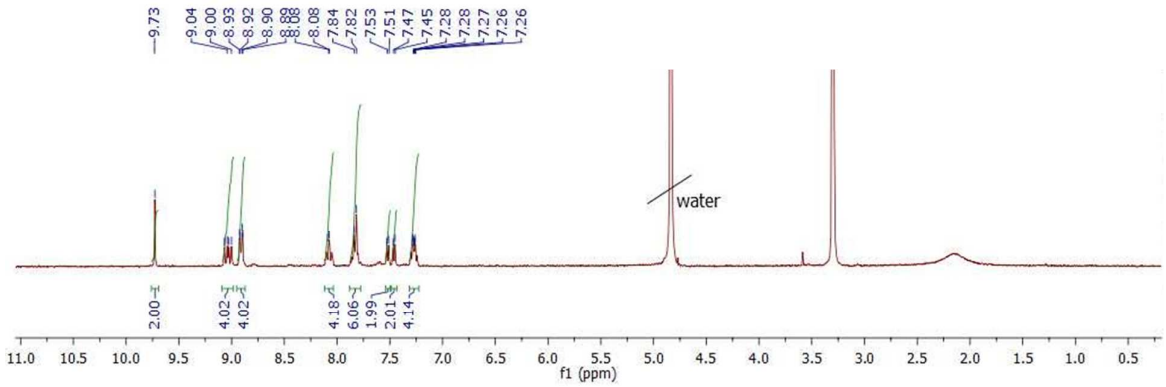

Figure S34. ^{1}H NMR spectrum of **FeL3-MC** in CD_3OD.

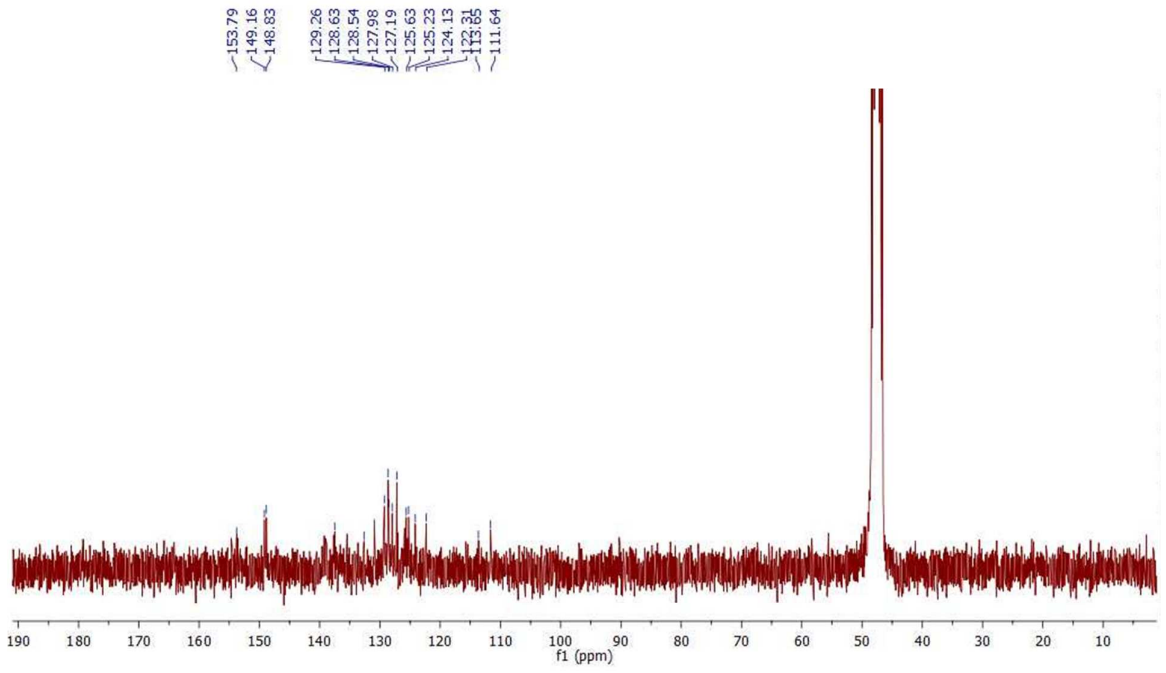

Figure S35. ^{13}C NMR spectrum of **FeL3-MC** in CD_3OD.

References

(1) Schärtl, W. *Light Scattering from Polymer Solutions and Nanoparticle Dispersions*. Springer Berlin Heidelberg: 2007.

(2) Arndt, K.-F.; Müller, G. *Polymercharakterisierung*. Carl Hanser Verlag, München Wien: 1996.

(3) Zimm, B. H. Apparatus and Methods for Measurement and Interpretation of the Angular Variation of Light Scattering; Preliminary Results on Polystyrene Solutions. *J. Chem. Phys.* **1948,** *16,* 1099-1116.

(4) Röder, T.; Morgenstern, B. The influence of activation on the solution state of cellulose dissolved in N-methylmorpholine-N-oxide-monohydrate. *Polymer* **1999,** *40,* 4143-4147.

(5) Burchard, W. In *Light Scattering from Polymers*; Springer Berlin Heidelberg: Berlin, Heidelberg, 1983; Vol. 48, pp 1-124.

(6) Guinier, A.; Fournet, G. *Small angle scattering of X-rays*. John Wiley & Sons, New York: 1955.

(7) Wesslau, V. H. Zur kenntnis von acrylsäure enthaltenden copolymerdispersionen. I. Über die auswertung von streulichtmessungen. *Makromol. Chem.* **1963,** *69,* 213-219.